

## Article

# Enhanced Adsorptive Removal of Dyes Using Mandarin Peel Biochars via Chemical Activation with $\text{NH}_4\text{Cl}$ and $\text{ZnCl}_2$

Hyunjun Park <sup>1</sup>, Jiseok Kim <sup>1</sup>, Yong-Gu Lee <sup>1,\*</sup>  and Kangmin Chon <sup>1,2,\*</sup> 

<sup>1</sup> Department of Environmental Engineering, College of Engineering, Kangwon National University, Kangwondaehak-gil, 1, Chuncheon-si 24341, Gangwon-do, Korea; hjpark1597@naver.com (H.P.); skyjskim95@gmail.com (J.K.)

<sup>2</sup> Department of Integrated Energy and Infra System, Kangwon National University, Kangwondaehak-gil, 1, Chuncheon-si 24341, Gangwon-do, Korea

\* Correspondence: yglee19@kangwon.ac.kr (Y.-G.L.); kmchon@kangwon.ac.kr (K.C.); Tel.: +82-33-250-6352 (K.C.)

**Abstract:** This study examined differences in the adsorption kinetics, isotherms, and thermodynamics of the dyes (methyl orange and fast green FCF) by pristine (M-biochar) and chemical activated mandarin peel biochars (MN-biochar and MZ-biochar). The specific surface area ( $1085.0 \text{ m}^2/\text{g}$ ) and pore volume ( $0.194 \text{ cm}^3/\text{g}$ ) of MZ-biochar much higher than those of the M-biochar (specific surface area =  $8.5 \text{ m}^2/\text{g}$ , pore volume =  $0.016 \text{ cm}^3/\text{g}$ ) and MN-biochar (specific surface area =  $181.1 \text{ m}^2/\text{g}$ , pore volume =  $0.031 \text{ cm}^3/\text{g}$ ). The equilibrium adsorption capacities (mg/g) of MO and FG using M-biochar (MO = 0.95, FG = 0.78) MN-biochar (MO = 2.52, FG = 2.13), and MZ-biochar (MO = 16.27, FG = 12.44) have well-matched the pseudo-second-order model ( $R^2 \geq 0.952$ ) compared with the pseudo-first-order model ( $R^2 \geq 0.008$ ). Furthermore, the better explanation of the adsorption behavior of dyes by the Freundlich isotherm model ( $R^2 \geq 0.978$ ) than the Langmuir isotherm model ( $R^2 \geq 0.881$ ) supports the assumption that the multilayer adsorption governed the adsorption of dyes using mandarin peel biochars. The adsorptions of dyes were significantly dependent on the solution pH and temperature since the electrostatic and spontaneous endothermic reactions governed their removal using the pristine and chemical activated mandarin peel biochars.

**Keywords:** adsorption; ammonium chloride; biochar; dyes; fast green FCF; mandarin peel; methyl orange; zinc chloride



**Citation:** Park, H.; Kim, J.; Lee, Y.-G.; Chon, K. Enhanced Adsorptive Removal of Dyes Using Mandarin Peel Biochars via Chemical Activation with  $\text{NH}_4\text{Cl}$  and  $\text{ZnCl}_2$ . *Water* **2021**, *13*, 1495. <https://doi.org/10.3390/w13111495>

Academic Editor: Antonio Zuorro

Received: 30 April 2021

Accepted: 24 May 2021

Published: 27 May 2021

**Publisher's Note:** MDPI stays neutral with regard to jurisdictional claims in published maps and institutional affiliations.



**Copyright:** © 2021 by the authors. Licensee MDPI, Basel, Switzerland. This article is an open access article distributed under the terms and conditions of the Creative Commons Attribution (CC BY) license (<https://creativecommons.org/licenses/by/4.0/>).

## 1. Introduction

Rapid population growth after the industrial revolution led to the development of the textile, cosmetics, paper, leather, and pharmaceutical industries. This significantly increased industrial wastewater discharge, causing serious water pollution [1,2]. Dyes are widely used in various industries (e.g., textiles and food) [3,4]. Textile and food wastewater with a high concentration of dyes can contaminate waterbodies, resulting in the reduction of light transmission to aquatic plants, thereby causing a reduction of photosynthesis. In addition, the dyes may have harmful effects on the aquatic ecosystem owing to the generation of aromatic amines that cause mutations in aquatic organisms. These mutations are a consequence of the aromatic amines being reduced upon contact with air [5,6]. Conventional biological wastewater treatment is ineffective for treating dyes wastewater because it causes a low ratio of biological oxygen demand to chemical oxygen demand (BOD/COD) from the aromatic structural compound of dyes that are not readily biodegradable [7,8]. In addition, the coagulation/flocculation treatment, which is a physicochemical process, is ineffective for the removal of soluble dyes [2]. Although the ozone treatment process can effectively remove soluble dyes, it is not economical because it requires a continuous ozone supply because of the short half-life for ozone [9]. Adsorption treatments might remove soluble dyes at a reduced cost compared to other treatment processes without producing reaction

by-products [10]. Various modern adsorbent materials, such as carbon nanotubes [11], graphene oxide [12], magnetic metal nanoparticles [13], Mxenes [14], and biopolymers [15], have been used for efficient removal of dyes from aqueous solutions. Yao et al. (2011) reported efficient methyl orange adsorption on multiwalled carbon nanotubes [11]. Yang et al. demonstrated high methylene blue adsorption on graphene oxide [12]. Yao et al. (2011) fabricated magnetic graphene oxides with metallic nanoparticles for methylene blue adsorption [13]. Additionally, Vakili et al. (2019, 2020) synthesized MXene based adsorbent for removal of methylene blue (the adsorption capacity = 209 mg/g) and examined the elimination efficiency of anionic dye from aqueous solutions using the combination of chitosan and activated carbon adsorbents (the adsorption capacity = 666 mg/g) [14,15]. Despite the advantages of these modern materials, including high efficiency, fast, and reusability, they may have harmful effects on living organisms in aquatic ecosystems due to their permeability to various organs and non-degradation under natural conditions. In addition, activated carbon has a high production cost when used as a representative adsorbent. It is also difficult to regenerate at the wastewater treatment plant scale. Therefore, it is necessary to develop an alternative adsorbent for dye wastewater treatment [16].

Biochar is a carbon-rich material with porous structures produced by the pyrolysis of agricultural and livestock biomass residues under oxygen-free conditions. They have the advantages of cost-effectiveness, renewability, reducing secondary environmental pollution, and creating high-value-added adsorbents [17]. Furthermore, when biochar is used as an adsorbent, the discharge of carbon dioxide (a gas contributing to global warming) into the atmosphere is reduced [18,19]. However, biochars compared to activated carbon, have comparatively smaller pore volume and surface areas. Therefore, chemical activation methods using activating chemicals, such as zinc chloride ( $\text{ZnCl}_2$ ) and ammonium chloride ( $\text{NH}_4\text{Cl}$ ), may improve biochar surface structure properties and adsorption capacity [20,21]. Ahiduzzamand and Sadrul Islam reported that the specific surface area of chemical-activated porous biochar using  $\text{ZnCl}_2$  ( $645 \text{ m}^2/\text{g}$ ) was approximately 23 times larger than that of pristine porous biochar ( $28 \text{ m}^2/\text{g}$ ) [21].

Globally, yearly mandarin production is approximately 100 million metric tons [22]. Its consumption generates large volumes of fruit peel as biomass waste [23]. Mandarin peels contain organic carbon components such as cellulose, hemicellulose, and pectin, which render them suitable for the production of environmentally friendly biochars through pyrolysis, which results in a material with excellent adsorption capacity [20]. Unugul and Nigiz. (2020) have achieved a complete copper removal using an acid-treated carbonized mandarin peel adsorbent [24]. However, a comprehensive study on the influence of the physicochemical characteristics of mandarin peel biochars via chemical activation on the removal of dyes in solutions has not yet been published.

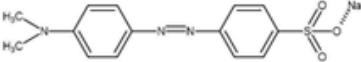
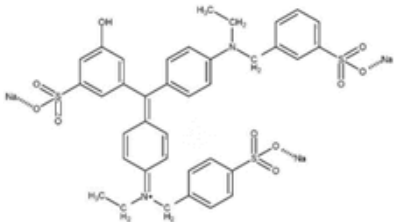
This study evaluates the influence of chemical activation with  $\text{NH}_4\text{Cl}$  and  $\text{ZnCl}_2$  on the adsorption of methyl orange (MO) and fast green FCF (FG) using mandarin peel biochars. The physicochemical properties of pristine (M-biochar) and chemically activated biochars with  $\text{NH}_4\text{Cl}$  (MN-biochar) and  $\text{ZnCl}_2$  (MZ-biochar) were characterized. The optimum adsorbent dosages, adsorption kinetics, and adsorption isotherm models of MO and FG were identified. Furthermore, various adsorption experiments were conducted to examine the influence of solution pH and temperature on the removal efficiencies of MO and FG in association with the physicochemical properties of mandarin peel biochars.

## 2. Materials and Methods

### 2.1. Reagents and Chemicals

All chemicals used in this study were of analytical grade. Dyes (i.e., MO and FG),  $\text{NH}_4\text{Cl}$ ,  $\text{ZnCl}_2$ , sodium hydroxide (NaOH), and hydrochloric acid (HCl) were purchased from DaeJung Chemicals (Siheung-si, Gyeonggi-do, Korea). Deionized (DI) water (resistivity  $> 18.2 \text{ M}\Omega \text{ cm}^{-1}$ , Barnstead Nanopure Water System, Lake Balboa, CA, USA) was used to prepare the standard solutions of MO and FG (concentration of each dye = 10 mg/L). The structures of MO and FG are listed in Table 1.

**Table 1.** Structure of the dyes.

	Methyl Orange	Fast Green FCF
Structure <sup>a</sup>		

<sup>a</sup> ChemAxon (<http://www.chemicalize.org>, accessed on 2 January 2021).

## 2.2. Preparation of Mandarin Peel Biochars

Mandarin was purchased from a local grocery store on Jeju Island (Jeju-do, Republic of Korea) and then separated into flesh and peels. The mandarin peels were rinsed with DI water three times to remove impurities and dried in an oven at 105 °C for 24 h. The dried mandarin peel was then crushed using a food grinder. For chemical activation with NH<sub>4</sub>Cl and ZnCl<sub>2</sub>, 1 g of dried mandarin peel was mixed with each activation chemical at a weight ratio (*w/w%*) of 1:1 using 2 mL of DI water. The mixed samples were then dried in an oven at 105 °C for 24 h. The pristine and chemically activated mandarin peel samples were crushed again with a food grinder. Subsequently, the pristine and chemically activated mandarin peels were then pyrolyzed using a tubular furnace (PyroTech, Namyangju-si, Gyeonggi-do, Korea) under the same conditions. The tubular furnace was heated to 700 °C at 5 °C min<sup>-1</sup> using N<sub>2</sub> gas (flow rate = 0.5 L min<sup>-1</sup>) and then maintained at that temperature for 6 h. After cooling to room temperature (20 ± 0.5 °C), the M-biochar, MN-biochar, and MZ-biochar were rinsed with DI water four times, filtered with glass fiber filters (GF/F, nominal pore size = 0.7 μm; Whatman, Clifton, NJ, USA), and then dried in an oven at 105 °C for 12 h. The M-biochar, MN-biochar, and MZ-biochar were subsequently homogenized using a 0.154 mm (100 mesh) sieve and then stored in a desiccator before use.

## 2.3. Characterization of Mandarin Peel Biochars

The elemental contents of the M-biochar, MN-biochar, and MZ-biochar were analyzed using an elemental analyzer (EuroEA3000 CHNS-O, EuroVector S.p.A, Milan, Italy). The atomic ratios of H/C and [(N/C) + (O/C)] might be used as indices to predict the aromaticity and polarity of the M-biochar, MN-biochar, and MZ-biochar [25]. The surface functional groups of the M-biochar, MN-biochar, and MZ-biochar were investigated using Fourier-transform infrared spectroscopy (ATR-FTIR; Frontier Optica, Perkin Elmer, Waltham, MA, USA) in the wavenumber range of 4000–700 cm<sup>-1</sup>. The biochars' point of zero charges (PZC) were evaluated using a surface zeta potential analyzer (Zetasizer Nano ZSP, Malvern, UK) at pH 1–11. The average pore diameter and specific surface area were measured using a Brunauer Emmett Teller analyzer (BELSORP-mini II, MicrotracBEL, Osaka, Japan). The total pore volume was calculated using the Barrett–Joyner–Halenda (BJH) method [26]. The M-biochar, MN-biochar, and MZ-biochar were degassed in a vacuum at 473 K during 48 h, and their N<sub>2</sub> adsorption-desorption isotherms were examined at 77.3 K in the relative pressure (*P/P*<sub>0</sub>) from 0.01 to 0.99.

## 2.4. Batch Adsorption Experiments

### 2.4.1. Optimal Adsorbent Dosages

The optimum dosages of M-biochar, MN-biochar, and MZ-biochar for MO and FG were determined. The adsorbents dosage (0.1–3 g/L) of M-biochar, MN-biochar, and MZ-biochar were added to 25 mL of the MO and FG solutions (initial concentration of each dye = 10 mg/L, pH = 7.0) in Erlenmeyer flasks. The sample solutions were then stirred at 160 rpm and 25 °C for 1 h using a shaking incubator (VS-8480, Vision Scientific, Daejeon, Republic of Korea). All experiments were performed in triplicate to minimize errors.

### 2.4.2. Adsorption Kinetics Experiments

For the adsorption kinetics, the optimal dosage of pristine and chemical activated mandarin peel biochars for MO (1.5 g/L) and FG (2.0 g/L) was added to 25 mL of sample solutions (initial concentration of each dye = 10 mg/L, pH = 7.0). The sample solutions were stirred at 160 rpm and 25 °C for 0–3 h in a shaking incubator. Subsequent to the batch adsorption experiments, the sample solutions were filtered using a GF/F. The concentrations of MO and FG at the initial and equilibrium states were measured using a UV-Vis spectrophotometer (UV-1280, Shimadzu, Kyoto, Japan) at UV absorbances of 460 and 625 nm, respectively [27,28]. All adsorption experiments were repeated three times to minimize errors. The amount of MO and FG solution adsorbed per unit of mass adsorbent,  $Q_t$  (mg/g), was calculated using the following equation [29]:

$$Q_t = \frac{(C_0 - C_e)V}{m} \quad (1)$$

where  $C_0$  and  $C_e$  denote the initial and equilibrium concentrations (mg/L) of MO and FG solutions, respectively,  $V$  is the volume (L) of the solution, and  $m$  is the mass (g) of the M-biochar, MN-biochar, and MZ-biochar.

The removal efficiencies of the MO and FG solutions were calculated using Equation (2):

$$\text{Removal efficiency (\%)} = \frac{(C_0 - C_e)V}{C_0} \times 100 \quad (2)$$

where  $C_e$  denotes the MO and FG concentrations (mg/L) at the equilibrium of the solutions.

The adsorption kinetics and capacities of MO and FG by M-biochar, MN-biochar, and MZ-biochar were determined using Equations (3) and (4) [30]:

$$\text{Pseudo-first-order model : } \ln(Q_e - Q_t) = \ln Q_e - k_1 t \quad (3)$$

$$\text{Pseudo-second-order-model : } \frac{t}{Q_t} = \frac{1}{k_2 Q_e^2} + \frac{1}{Q_e} t \quad (4)$$

where  $Q_e$  and  $Q_t$  are the amount of dyes adsorbed per unit mass of the adsorbent (mg/g) at equilibrium and time  $t$ , respectively.  $k_1$  (1/h) is the constant of the pseudo-first-order equation, and  $k_2$  (g/mg·h) denotes the pseudo-second-order equation constant.

### 2.4.3. Adsorption Isotherm Experiments

The adsorption isotherms of MO and FG by M-biochar, MN-biochar, and MZ-biochar were obtained using different initial concentrations for the MO and FG solutions (1–80 mg/L). Each mandarin peel biochar (i.e., M-biochar, MN-biochar, and MZ-biochar) was added at 1.5 g/L to the MO solution and at 2.0 g/L to the FG solution under controlled conditions (agitation speed = 160 rpm, contact time = 1 h, pH = 7.0, and temperature = 25 °C). The adsorption isotherm results were determined using Langmuir and Freundlich isotherm models. The Langmuir isotherm model was defined as the following Equation (5) [31]:

$$\text{Langmuir isotherm : } Q_e = Q_{max} \frac{K_L C_e}{1 + K_L C_e} \quad (5)$$

where  $C_e$  (mg/L) is the equilibrium concentration of the MO and FG,  $Q_{max}$  (mg/g) is the maximum monolayer adsorption capacity of MO and FG, and  $K_L$  (L/mg) is the equilibrium constant of the Langmuir isotherm model.

The Freundlich isotherm model was expressed as follows [32]:

$$\text{Freundlich isotherm : } Q_e = K_F C_e^{1/n} \quad (6)$$

where  $K_F$  (mg<sup>1-(1/n)</sup>L<sup>1/n</sup>/g) and  $n$  (dimensionless) are the constants associated with the relative maximum adsorption capacity and adsorption intensity, respectively.

#### 2.4.4. Influence of Solution Temperature and pH on Adsorption of Dyes

The influence of solution temperature and pH on the adsorption of MO and FG by the pristine and chemically activated mandarin peel biochars were investigated at various temperatures (15–35 °C) and pH (3.0–9.0) conditions (initial concentration of each dye = 10 mg/L, agitation speed = 160 rpm, contact time = 1 h). The solution pH was adjusted using 0.1 N HCl and 0.1 N NaOH. The removal efficiencies of MO and FG using M-biochar, MN-biochar, and MZ-biochar were calculated using Equation (2).

The thermodynamic parameters of MO and FG adsorption were calculated using the following Equations (7)–(9) [33]:

$$K_d = \frac{Q_e}{C_e} \quad (7)$$

$$\Delta G^\circ = -RT \ln(K_d) \quad (8)$$

$$\ln(K_d) = \frac{\Delta S^\circ}{R} - \frac{\Delta H^\circ}{RT} \quad (9)$$

where  $K_d$  (L/g) is the distribution coefficient.  $\Delta G^\circ$  (kJ/mol),  $\Delta H^\circ$  (kJ/mol), and  $\Delta S^\circ$  (kJ/mol·K) are the Gibbs free energy, enthalpy, and entropy, respectively.  $R$  is the ideal gas constant (8.314 J/mol·K), and  $T$  is the absolute temperature (K) of the aqueous solution.  $\Delta H^\circ$  and  $\Delta S^\circ$  were calculated from the slope and intercept in the linear graphs of  $\ln K_d$  and  $1/T$ , respectively.

### 3. Results and Discussions

#### 3.1. Physicochemical Characteristics of Mandarin Peel Biochars

SEM images of the M-biochar, MN-biochar, and MZ-biochar are shown in Figure 1. Figure 1a revealed various shapes of macropores and open spaces that give the M-biochar an adsorption ability to MO and FG. However, the pores might be improved and further enhanced by chemical activation during the etching reaction by  $\text{NH}_4\text{Cl}$  and  $\text{ZnCl}_2$ , which results in the formation of some pores as presented in Figure 1b,c [34]. Therefore it effectively improved the specific surface areas and increased the pore properties as summarized in Table 2.

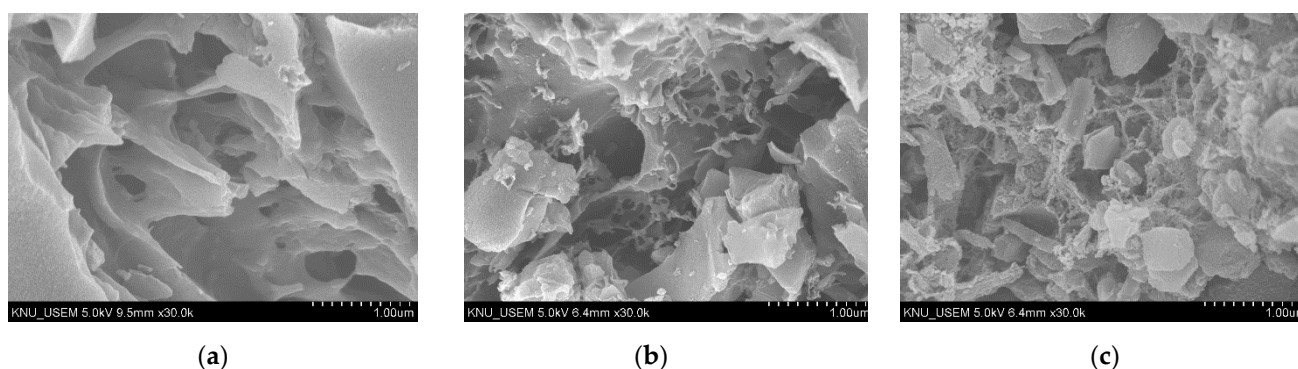


**Figure 1.** The SEM images of (a) M-biochar, (b) MN-biochar, and (c) MZ-biochar.

The physicochemical properties (i.e., BET isotherms, bulk elements, the atomic molar ratio, specific surface area, total pore volume, and pore size) of the M-biochar, MN-biochar, and MZ-biochar are presented in Figure 2 and Table 2. The  $\text{N}_2$  adsorption-desorption isotherms of the M-biochar, and MN-biochar and MZ-biochar corresponded to Type II and Type IV, respectively. The Type II isotherms are expected to govern monolayer adsorption at relatively low-pressure states, and the multilayer adsorption primarily occurred at relatively high-pressure states (Figure 2a). The Type IV isotherms are determined by the monolayer-multilayer adsorption on the mesopore walls and the interactions between the molecules in the condensed state (Figure 2b,c) [35]. In the case of Figure 2b, capillary condensation is occurred by hysteresis when the pore width exceeds a certain critical width.

The MZ-biochar showed considerably larger specific surface area ( $1085.0 \text{ m}^2/\text{g}$ ) and total pore volume ( $0.19 \text{ cm}^3/\text{g}$ ) compared to those values from the M-biochar (specific surface area =  $8.5 \text{ m}^2/\text{g}$ , total pore volume =  $0.016 \text{ cm}^3/\text{g}$ ) and MN-biochar (specific surface area =  $181.1 \text{ m}^2/\text{g}$ , total pore volume =  $0.031 \text{ cm}^3/\text{g}$ ). However, the average diameter of the MZ-biochar pores ( $3.62 \text{ nm}$ ) was smaller than those of the M-biochar ( $8.74 \text{ nm}$ ) and the MN-biochar ( $4.58 \text{ nm}$ ). These observations indicate that chemical activation with  $\text{ZnCl}_2$  of M-biochar was more effective in improving the surface and pore properties than the chemical activation with  $\text{NH}_4\text{Cl}$  of M-biochar [36,37]. In addition, the mesoporous structures of the mandarin peel biochars may govern the adsorption of MO and FG [20]. The H/C and [(O/C) + (N/C)] values corresponded to the aromaticity and polarity of the mandarin peel biochars, respectively. The smaller the H/C molar ratio meant, the greater the aromaticity. Although the polarity of the M-biochar was comparatively larger than that of the MN-biochar and MZ-biochar ( $0.070$  (M-biochar)  $>$   $0.065$  (MN-biochar)  $>$   $0.050$  (MZ-biochar)), the aromaticity of the M-biochar was smaller compared to the MN-biochar and MZ-biochar ( $0.26$  (MN-biochar)  $>$   $0.27$  (MZ-biochar)  $>$   $0.29$  (M-biochar)). These results suggest that the MN-biochar and MZ-biochar were more carbonized than the M-biochar.

**Table 2.** The physicochemical properties of M-biochar, MN-biochar, and MZ-biochar.

	M-Biochar	MN-Biochar	MZ-Biochar
C (%)	$79.53 \pm 0.71$	$80.05 \pm 0.55$	$79.21 \pm 0.46$
H (%)	$1.92 \pm 0.015$	$1.72 \pm 0.028$	$1.78 \pm 0.040$
O (%)	$5.09 \pm 0.078$	$4.88 \pm 0.061$	$3.63 \pm 0.089$
N (%)	$2.07 \pm 0.019$	$1.76 \pm 0.023$	$1.44 \pm 0.029$
S (%)	$0.13 \pm 0.010$	$0.25 \pm 0.037$	$0.15 \pm 0.011$
H/C	$0.29 \pm 0.003$	$0.26 \pm 0.002$	$0.27 \pm 0.003$
O/C	$0.048 \pm 0.008$	$0.046 \pm 0.009$	$0.034 \pm 0.010$
N/C	$0.022 \pm 0.003$	$0.019 \pm 0.001$	$0.016 \pm 0.002$
Specific surface area ( $\text{m}^2/\text{g}$ )	8.5	181.1	1085.0
Total pore volume ( $\text{cm}^3/\text{g}$ )	0.016	0.031	0.19
Pore size (nm)	8.74	4.58	3.62

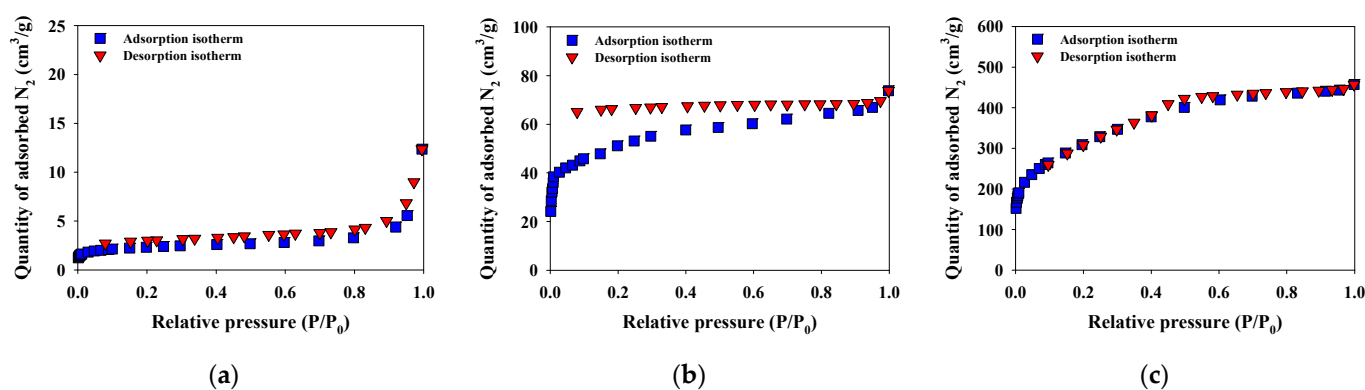


**Figure 2.**  $\text{N}_2$  adsorption-desorption isotherms of (a) M-biochar, (b) MN-biochar, and (c) MZ-biochar.

The functional group compositions of the M-biochar, MN-biochar, and MZ-biochar are shown in Figure 3. The O–H stretching of alcohols ( $3570\text{--}3200 \text{ cm}^{-1}$ ), the C=O stretching of carbonyls ( $1570\text{--}1515 \text{ cm}^{-1}$ ), and C–O stretching of alcohols ( $1075\text{--}1000 \text{ cm}^{-1}$ ) were commonly detected in M-biochar, MN-biochar, and MZ-biochar [38,39]. These IR peaks are associated with the components of the mandarin peel, such as C, H, O, and N (Table 2). Nevertheless, a new IR peak related to the C–O stretching of alcohols was observed for the MN-biochar and MZ-biochar in the range of  $1200\text{--}1100 \text{ cm}^{-1}$  [40]. These results imply that chemical activation may significantly influence the composition of functional groups of biochars related to the MO and FG adsorption capacity [41]. Variations in the surface

zeta potential (mV) of the M-biochar, MN-biochar, and MZ-biochar as pH values of the solution are presented in Figure 4. The surface zeta potential of the M-biochar, MN-biochar, and MZ-biochar varied depending on the solution pH. The PZC of M-biochar, MN-biochar, and MZ-biochar were extrapolated from the experimental results of the surface zeta potential and were found to be pH 2.9, 2.4, and 3.0, respectively. This implies that the pH value of the solution is a critical factor that affects the physical parameters of the MO ( $pK_a = 3.58$ ) and FG ( $pK_a = 3.11$ ). Furthermore, it is directly influential on the surface charge and the adsorption ability of the mandarin peel biochars [40].

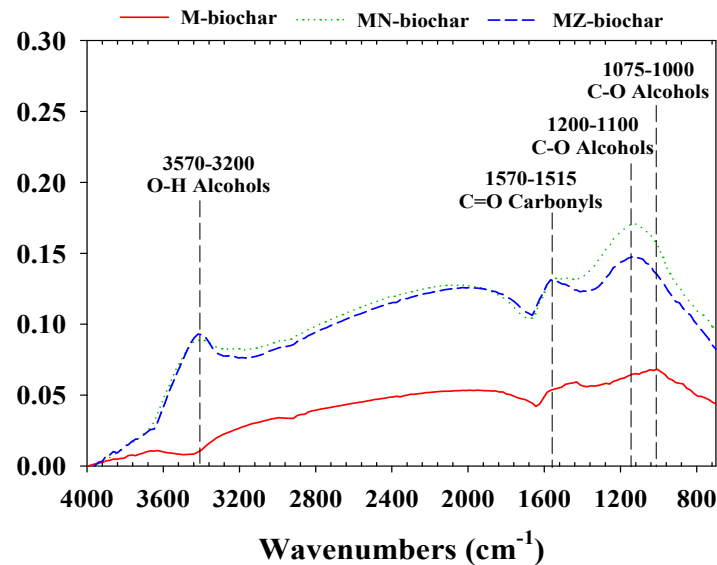


Figure 3. The ATR-FTIR spectra of M-biochar, MN-biochar, and MZ-biochar.

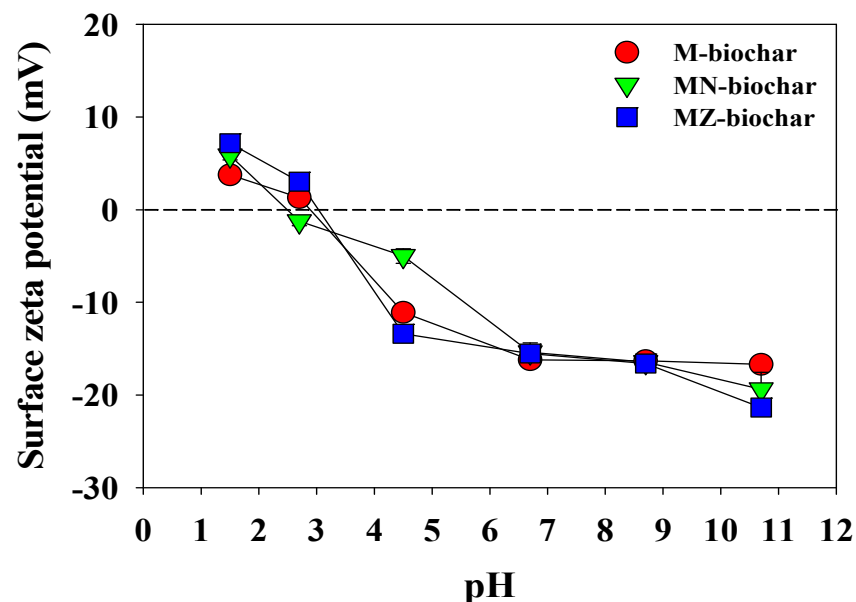
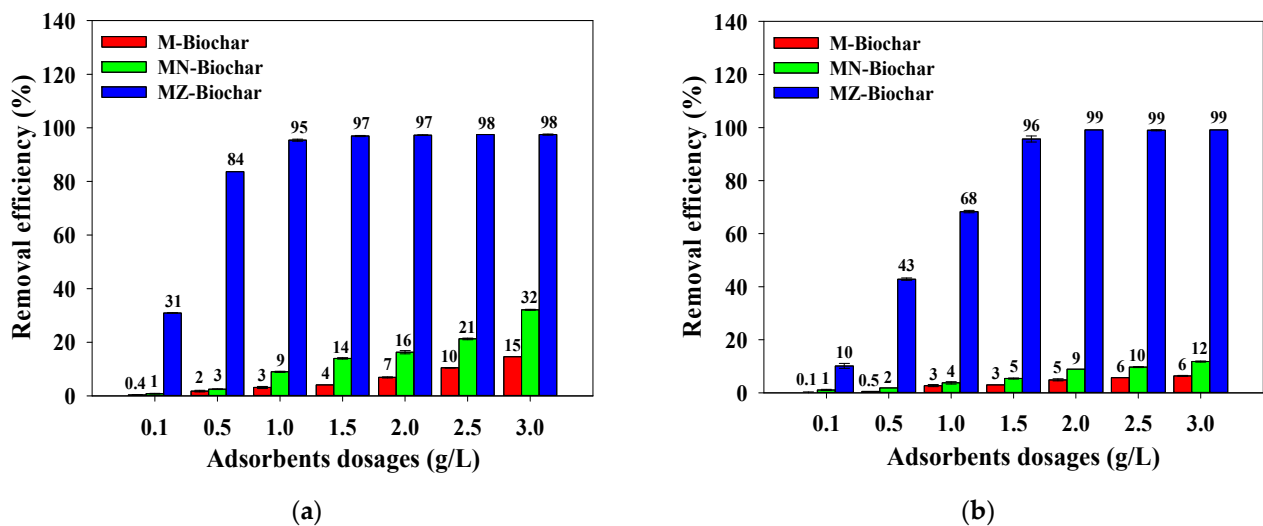


Figure 4. Surface zeta potential of the M-biochar, MN-biochar, and MZ-biochar ( $n = 3$ ).

### 3.2. Influence of Mandarin Peel Biochar Dosage

The changes in the removal efficiencies of MO and FG are shown with the corresponding adsorbent dosages in Figure 5. The removal efficiencies of MO and FG were enhanced with increasing dosages of the pristine and chemically activated mandarin biochars. The removal efficiencies of MO and FG by MZ-biochar were much greater than those of M-biochar and MN-biochar (MZ-biochar > MN-biochar > M-biochar). This suggests that the

difference in the specific surface areas of the mandarin peel biochars (the specific surface area depends on the chemical activation) might influence the adsorption capacities of MO and FG [42]. The removal efficiencies of MO achieved a steady-state at an MZ-biochar dosage of 1.5 g/L (removal efficiency of MO = 97%). The FG was at a steady-state removal efficiency at the MZ-biochar dosage of 2.0 g/L (removal efficiency of FG = 99%). Consequently, the pristine and chemically activated mandarin peel biochar dosages for MO and FG were applied for the following adsorption experiments at 1.5 and 2.0 g/L, respectively.



**Figure 5.** The influence of adsorbent doses on the removal efficiency of the MO and FG using M-biochar, MN-biochar, and MZ-biochar: (a) MO and (b) FG ( $C_0 = 10$  mg/L; agitation speed = 160 rpm; contact time = 1 h; pH = 7.0; temperature = 25 °C,  $n = 3$ ).

### 3.3. Adsorption Kinetics of Dyes

Figure 6 shows the adsorption kinetics of MO and FG by M-biochar, MN-biochar, and MZ-biochar. Both MO and FG adsorptions using MZ-biochar rapidly reached equilibrium at 0.5 h. These observations may explain that the difference in specific surface area (MZ-biochar = 1085.0 m<sup>2</sup>/g > MN-biochar = 181.1 m<sup>2</sup>/g > M-biochar = 8.5 m<sup>2</sup>/g) on the adsorption capacity of MZ-biochar has a critical role in the adsorption of MO and FG [43]. Table 3 presents the adsorption kinetic parameters for MO and FG adsorption using pristine and chemically activated mandarin peel biochars. The adsorption kinetics of MO and FG on both the pristine and chemically activated mandarin peel biochars showed good agreement with results from the pseudo-second-order model ( $R^2$  for MO: 0.980–0.999;  $R^2$  for FG: 0.952–0.999). The same comparison with results from the pseudo-first-order model showed inferior agreement ( $R^2$  for MO: 0.465–0.575;  $R^2$  for FG: 0.008–0.565). Furthermore, the equilibrium adsorption capacities of MO ( $Q_{e, cal} = 16.27$  mg/g) and FG ( $Q_{e, cal} = 12.45$  mg/g) by the MZ-biochars were greater than the equilibrium adsorption capacities of MO and FG by M-biochar ( $Q_{e, cal}$ : MO = 0.97 mg/g and FG = 0.80 mg/g) and MN-biochar ( $Q_{e, cal}$ : MO = 2.53 mg/g and FG = 2.22 mg/g). The greater  $Q_e$  values of MZ-biochar supported the assumption that MZ-biochar was more effective for removing MO and FG due to its significantly larger specific surface area than those of the M-biochar and MN-biochar.

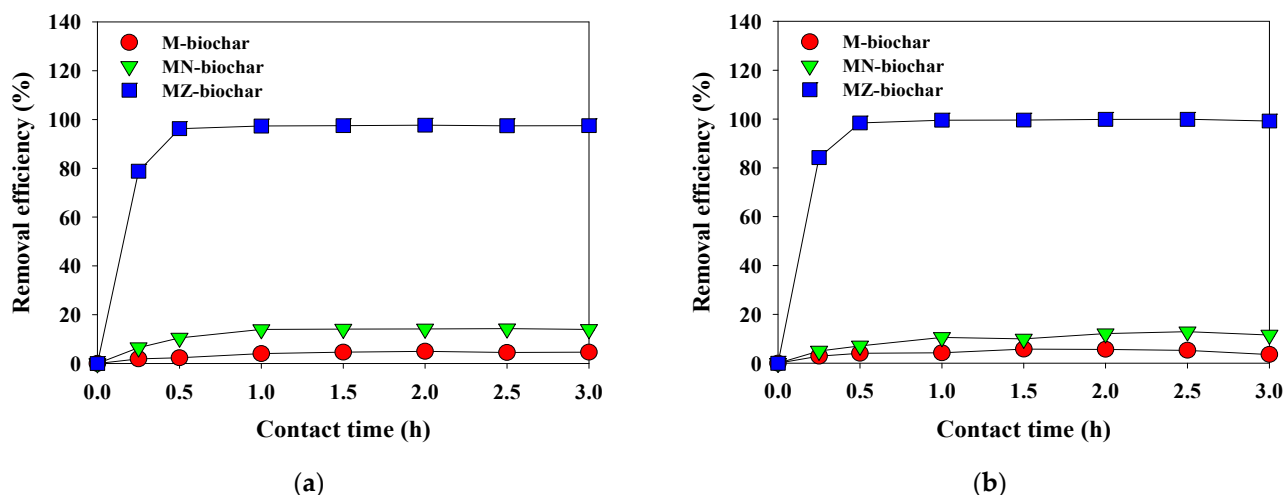


**Figure 6.** The kinetics for the removal efficiency of the MO and FG using M-biochar, MN-biochar, MZ-biochar: (a) MO and (b) FG ( $n = 3$ ;  $C_0 = 10$  mg/L; adsorbent dose for MO = 1.5 g/L, adsorbent dose for FG = 2.0 g/L; agitation speed = 160 rpm; pH = 7.0; temperature = 25 °C,  $n = 3$ ).

**Table 3.** The kinetic parameters for the removal of the MO and FG using M-biochar, MN-biochar and MZ-biochar ( $n = 3$ ).

Adsorbents Dyes		M-Biochar		MN-Biochar		MZ-Biochar	
		MO	FG	MO	FG	MO	FG
Pseudo-first- order	$Q_{e, exp}$ (mg/g)	$0.95 \pm 0.098$	$0.78 \pm 0.039$	$2.52 \pm 0.42$	$2.13 \pm 0.38$	$16.27 \pm 0.91$	$12.44 \pm 0.88$
	$Q_{e, cal}$ (mg/g)	$2.06 \pm 0.19$	$15.85 \pm 0.23$	$1.78 \pm 0.12$	$2.07 \pm 0.66$	$16.00 \pm 0.38$	$1.90 \pm 0.62$
	$k_1$ (1/h)	$0.49 \pm 0.057$	$0.063 \pm 0.004$	$0.56 \pm 0.092$	$0.48 \pm 0.083$	$0.063 \pm 0.009$	$0.52 \pm 0.017$
Pseudo-second- order	$R^2$	0.575	0.008	0.465	0.565	0.482	0.206
	$Q_{e, cal}$ (mg/g)	$0.97 \pm 0.10$	$0.80 \pm 0.022$	$2.53 \pm 0.28$	$2.22 \pm 0.67$	$16.27 \pm 0.096$	$12.45 \pm 0.88$
	$k_2$ (g/mg·h)	$2.81 \pm 0.19$	$3.14 \pm 0.44$	$3.45 \pm 0.58$	$0.98 \pm 0.020$	$12.56 \pm 0.29$	$12.81 \pm 0.23$
	$R^2$	0.981	0.962	0.996	0.952	0.999	0.999

### 3.4. Adsorption Isotherms of Dyes

The adsorption behaviors of the MO and FG using M-biochar, MN-biochar, and MZ-biochar are identified with the Langmuir and Freundlich isotherm models (Table 4). All mandarin peel biochars well fitted with the multilayer adsorption characteristics of the Freundlich isotherm model [44] than those of the Langmuir isotherm model, which was monolayer adsorption for MO and FG [45]. The  $n$  values (the dimensionless adsorption intensity) of the pristine and chemically activated mandarin peel biochars were used to evaluate the adsorption affinity toward MO and FG using the Freundlich isotherm model: (i)  $n > 1$  (favorable), (ii)  $n = 1$  (linear), and (iii)  $n < 1$  (unfavorable) [29]. The adsorption of MO by M-biochar ( $n = 4.71$ ), MN-biochar ( $n = 1.81$ ), and MZ-biochar ( $n = 1.68$ ), and the adsorption of FG by MZ-biochar ( $n = 1.38$ ) was favorable. However, the adsorption of FG by M-biochar ( $n = 0.96$ ) and MN-biochar ( $n = 0.98$ ) was unfavorable. Shin et al. (2020) explained that micropollutants were more adsorbed by chemical-modified biochar ( $n > 1$ ) compared to the pristine biochar ( $n < 1$ ) [46]. These results might explain the difference in the MO and FG adsorption affinities depending on the chemical activation.

**Table 4.** The isotherm parameters for the removal of the MO and FG using M-biochar, MN-biochar and MZ-biochar ( $n = 3$ ).

Adsorbents Dyes		M-Biochar		MN-Biochar		MZ-Biochar	
		MO	FG	MO	FG	MO	FG
Langmuir	$Q_{max}$ (mg/g)	$2.00 \pm 0.18$	$14.47 \pm 0.57$	$0.14 \pm 0.008$	$14.39 \pm 0.67$	$14.25 \pm 0.91$	$45.87 \pm 2.19$
	$K_L$ (L/mg)	$0.01 \pm 0.002$	$0.35 \pm 0.022$	$0.85 \pm 0.096$	$0.42 \pm 0.22$	$0.069 \pm 0.003$	$0.18 \pm 0.097$
	$R^2$	0.959	0.791	0.893	0.843	0.813	0.841
Freundlich	$n$	$4.71 \pm 0.39$	$0.96 \pm 0.019$	$1.81 \pm 0.57$	$0.98 \pm 0.44$	$1.68 \pm 0.096$	$1.38 \pm 0.022$
	$K_F$ (mg <sup>1-(1/n)</sup> L <sup>1/n</sup> /g)	$0.42 \pm 0.046$	$12.35 \pm 0.36$	$1.13 \pm 0.38$	$12.87 \pm 0.84$	$38.21 \pm 2.87$	$3.67 \pm 0.22$
	$R^2$	0.999	0.999	0.999	0.998	0.999	0.997

### 3.5. Influence of Temperature and pH on Adsorption of Dyes

The influence of temperature on the adsorption of MO and FG by the pristine and chemically activated mandarin peel biochars are compared in Figure 7. The removal efficiencies of MO and FG using M-biochar, MN-biochar, and MZ-biochar progressively improved with increasing temperature (15–35 °C). In particular, the adsorption capacities of MZ-biochars for MO and FG were significantly greater than those from the M-biochar and the MN-biochar. A possible explanation for these observations is that the adsorption of MO and FG onto M-biochar, MN-biochar, and MZ-biochar was endothermic [47].

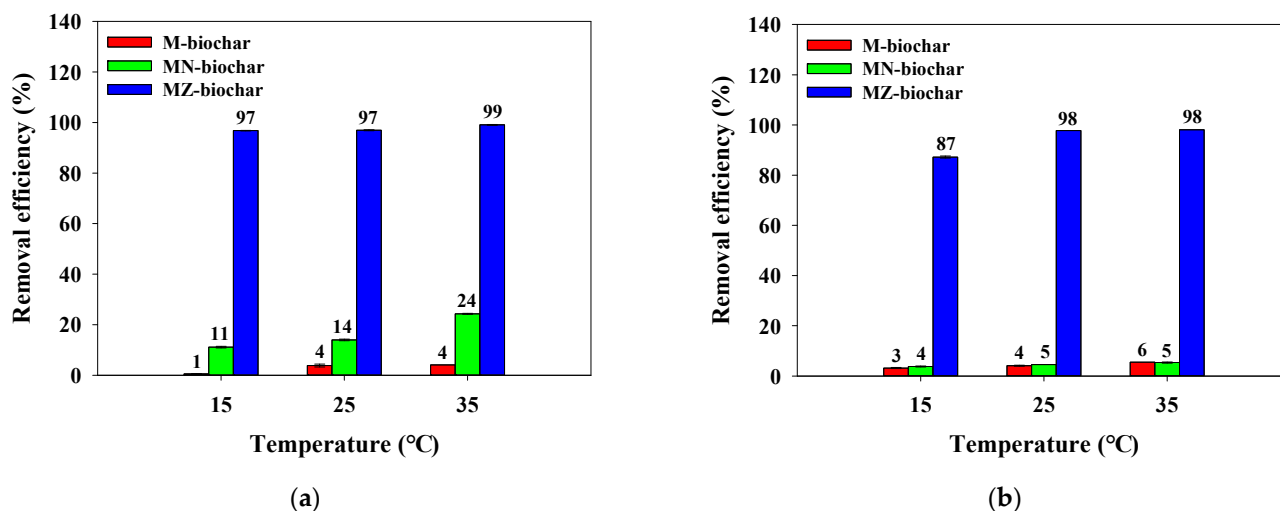


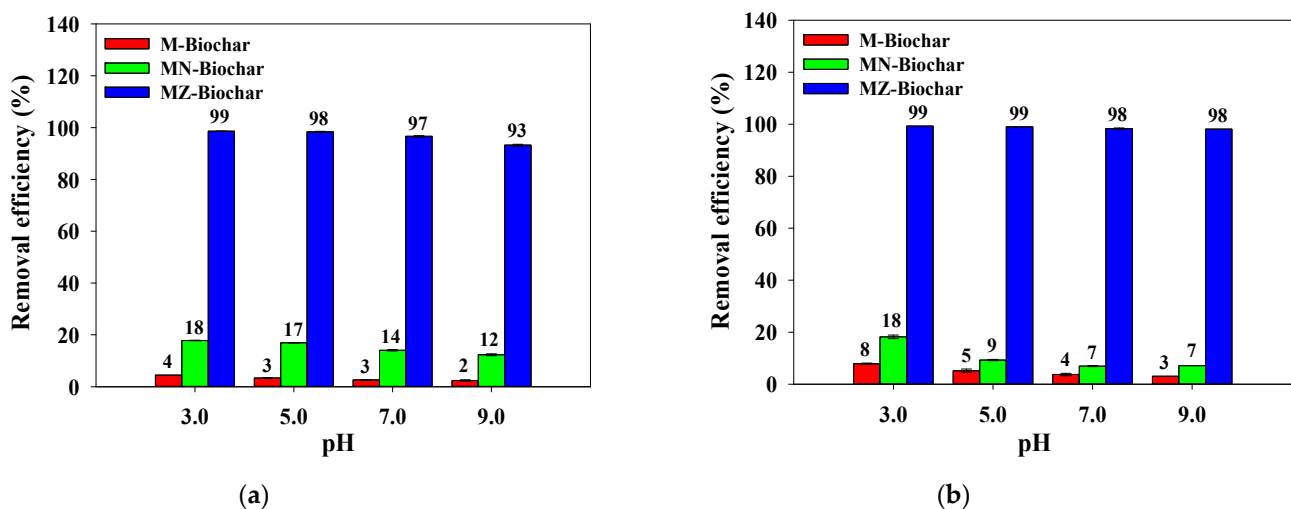
**Figure 7.** The influence of temperature on the removal efficiency of the MO and FG using M-biochar, MN-biochar, MZ-biochar: (a) MO and (b) FG ( $C_0 = 10$  mg/L; adsorbent dose for MO = 1.5 g/L, adsorbent dose for FG = 2.0 g/L; agitation speed = 160 rpm; contact time = 1 h; pH = 7.0,  $n = 3$ ).

The thermodynamic parameters (i.e.,  $\Delta G^\circ$ ,  $\Delta H^\circ$ , and  $\Delta S^\circ$ ) of MO and FG adsorption onto the pristine and chemically activated mandarin peel biochars are shown in Table 5. The negative  $\Delta G^\circ$  values indicated the spontaneous of MO and FG adsorption by M-biochar, MN-biochar, and MZ-biochar under the different temperatures [33]. The positive  $\Delta H^\circ$  values suggested that the adsorption of MO and FG onto the M-biochar (MO: 0.002 kJ/mol; FG: 0.008 kJ/mol), MN-biochar (MO: 0.050 kJ/mol; FG: 0.012 kJ/mol), and MZ-biochar (MO: 0.003 kJ/mol; FG: 0.002 kJ/mol) was endothermic in nature. Fan et al. (2016) reported that the  $\Delta H^\circ$  value of <40 kJ/mol might be attributed to physical adsorption [48]. Moreover, the positive  $\Delta S^\circ$  values indicated an increase in the randomness at the solid-solution interface during the MO and FG adsorption using M-biochar (MO: 0.032 kJ/mol·K; FG: 0.043 kJ/mol·K), MN-biochar (MO: 0.039 kJ/mol·K; FG: 0.052 kJ/mol·K), and MZ-biochar (MO: 0.045 kJ/mol·K; FG: 0.037 kJ/mol·K) [49].

The influence of pH (pH 3–9) on the adsorption of MO and FG for M-biochar, MN-biochar, and MZ-biochar are presented in Figure 8. The removal efficiency of MO and FG by M-biochar, MN-biochar, and MZ-biochar decreased as the pH increased. These results might be attributed to the electrostatic interaction between the positive-charged surface of mandarin peel biochars and the anionic dyes in strong acidic pH conditions (<pH 3) [50]. The removal efficiencies of the MO and FG by the M-biochar, MN-biochar, and MZ-biochar were in good agreement with the order of the Log D values (distribution coefficient) of the MO and FG under different pH conditions (pH 3.0 (MO: Log D = 2.53; FG: Log D = 1.18) > pH 5.0 (MO: Log D = 1.54; FG: Log D = 0.17) > pH 7.0 (MO: Log D = 1.30; FG: Log D = -0.04) > pH 9.0: (MO: Log D = 1.29; FG: Log D = -0.37)) (Supplementary Information, Table S1). Moreover, the removal efficiencies of MO and FG using MZ-biochar were greater than those of M-biochar and MN-biochar because of the specific surface area differences (MZ-biochar = 1085.0 m<sup>2</sup>/g > MN-biochar = 181.1 m<sup>2</sup>/g > M-biochar = 8.5 m<sup>2</sup>/g) [51].

**Table 5.** The thermodynamic parameters of MO and FG using the M-biochar, MN-biochar, and MZ-biochar ( $n = 3$ ).

Adsorbents	Dyes	Thermodynamic Parameters			
		Temperature (K)	$\Delta G^\circ$ (kJ/mol)	$\Delta H^\circ$ (kJ/mol)	$\Delta S^\circ$ (kJ/mol·K)
M-biochar	MO	288	$-2.84 \pm 0.17$	$0.002 \pm 0.0005$	$0.032 \pm 0.002$
		298	$-3.57 \pm 0.14$		
		308	$-4.35 \pm 0.11$		
	FG	288	$-4.24 \pm 0.09$	$0.008 \pm 0.0007$	$0.043 \pm 0.003$
		298	$-4.50 \pm 0.12$		
		308	$-4.81 \pm 0.10$		
MN-biochar	MO	288	$-5.59 \pm 0.21$	$0.050 \pm 0.001$	$0.039 \pm 0.009$
		298	$-5.80 \pm 0.34$		
		308	$-6.45 \pm 0.20$		
	FG	288	$-4.38 \pm 0.38$	$0.012 \pm 0.002$	$0.052 \pm 0.003$
		298	$-4.58 \pm 0.25$		
		308	$-4.75 \pm 0.28$		
MZ-biochar	MO	288	$-11.27 \pm 0.23$	$0.003 \pm 0.002$	$0.045 \pm 0.009$
		298	$-11.35 \pm 0.13$		
		308	$-12.86 \pm 0.42$		
	FG	288	$-9.69 \pm 0.33$	$0.002 \pm 0.0003$	$0.037 \pm 0.005$
		298	$-11.35 \pm 0.32$		
		308	$-11.75 \pm 0.25$		

**Figure 8.** The influence of pH on the removal efficiency of the MO and FG using M-biochar, MN-biochar, MZ-biochar: (a) MO and (b) FG ( $C_0 = 10$  mg/L; adsorbent dose for MO = 1.5 g/L, adsorbent dose for FG = 2.0/g; agitation speed = 160 rpm; contact time = 1 h; temperature = 25 °C,  $n = 3$ ).

#### 4. Conclusions

This study demonstrated that the adsorption capacity for MO and FG of mandarin peel biochar could be improved by pretreatment with  $\text{NH}_4\text{Cl}$  and  $\text{ZnCl}_2$ . Furthermore, the removal efficiency of the mandarin peel biochars varied greatly depending on the physicochemical properties of the MO and FG and biochars. There are five main conclusions from this study.

- Pretreatment with  $\text{ZnCl}_2$  was the most effective for increasing the specific surface area of mandarin peel biochars. Specific surface area was closely related to the adsorption of MO and FG (MZ-biochar ( $1085.0 \text{ m}^2/\text{g}$ ) > MN-biochar ( $181.1 \text{ m}^2/\text{g}$ ) > M-biochar ( $8.4 \text{ m}^2/\text{g}$ )).

- The adsorption of MO and FG using M-biochar, MN-biochar, and MZ-biochar was described better by the pseudo-second-order model for chemical adsorption ( $R^2 = 0.952\text{--}0.999$ ) than by the pseudo-first-order model ( $R^2 = 0.008\text{--}0.575$ ).
- The adsorption of MO and FG by M-biochar, MN-biochar, and MZ-biochar was better modeled by the Freundlich isotherm Equation ( $R^2 = 0.997\text{--}0.999$ ), with multilayer adsorption characteristics, than the Langmuir isotherm Equation ( $R^2 = 0.791\text{--}0.893$ ), which has monolayer adsorption characteristics.
- The correlation of temperature increases with increases of MO and FG removal efficiencies onto the pristine and chemical activated mandarin peel biochars indicated that the adsorption reaction was a spontaneous and endothermic reaction.
- The adsorption efficiencies of the dyes using the M-biochar, MN-biochar, and MZ-biochar in acidic pH conditions were effective compared with the neutral and alkali pH conditions. These results suggest that the mandarin peel biochars may be a promising option in improving the dye removal from a real-scale acidic wastewater treatment plant.

**Supplementary Materials:** The following are available online at <https://www.mdpi.com/article/10.3390/w13111495/s1>, Table S1: The physicochemical characteristics of the dyes.

**Author Contributions:** Conceptualization, H.P. and J.K.; methodology, H.P.; validation, J.K.; formal analysis, H.P.; data curation, J.K.; writing—original draft preparation, H.P. and J.K.; writing—review and editing, Y.-G.L. and K.C.; supervision, K.C.; funding acquisition, K.C. All authors have read and agreed to the published version of the manuscript.

**Funding:** This work was supported by the National Research Foundation of Korea (NRF) grant funded by the Korea government (MSIT) (No. 2020R1A4A1019568).

**Conflicts of Interest:** The authors declare no conflict of interest.

## Abbreviations

$C_e$	Concentration of dyes at equilibrium (mg/L)
$C_0$	Initial concentrations of dyes (mg/L)
$\Delta G^\circ$	The Gibbs free energy (kJ/mol)
$\Delta H^\circ$	The enthalpy (kJ/mol)
$\Delta S^\circ$	The entropy (kJ/mol·K)
FG	Fast Green FCF
$k_1$	Pseudo-first-order rate constant (1/h)
$k_2$	Pseudo-second-order rate constant (g/mg·hr)
$K_F$	Freundlich isotherm capacity factor ( $\text{mg}^{1-(1/n)} \text{L}^{1/n}/\text{g}$ )
$K_L$	The adsorption energy (L/mg)
$K_d$	The distribution coefficient (L/g)
$Q_e$	The quantities of the adsorbed dyes at equilibrium (mg/g)
$Q_t$	The amounts of the adsorbed dyes at time t (mg/g)
$Q_{e, \text{exp}}$	The adsorption capacities of the dyes at equilibrium (mg/g)
$Q_{\text{max}}$	The maximum adsorption capacity (mg/g)
M-biochar	Pristine mandarin peel biochar
MN-biochar	$\text{NH}_4\text{Cl}$ activated mandarin peel biochar
MZ-biochar	$\text{ZnCl}_2$ activated mandarin peel biochar
MO	Methyl orange
n	The adsorption affinity of dyes
T	The absolute temperature (K)
V	Volume of dyes solution (L)

## References

1. Namasivayam, C.; Muniasamy, N.; Gayatri, K.; Rani, M.; Ranganathan, K. Removal of dyes from aqueous solutions by cellulosic waste orange peel. *Bioresour. Technol.* **1996**, *57*, 37–43. [[CrossRef](#)]
2. El-Sayed, G.O. Removal of methylene blue and crystal violet from aqueous solutions by palm kernel fiber. *Desalination* **2011**, *272*, 225–232. [[CrossRef](#)]
3. Stolz, A. Basic and applied aspects in the microbial degradation of azo dyes. *Appl. Microbiol. Biotechnol.* **2001**, *56*, 69–80. [[CrossRef](#)] [[PubMed](#)]
4. Mittal, A.; Kaur, D.; Mittal, J. Batch and bulk removal of a triarylmethane dye, fast green FCF, from wastewater by adsorption over waste materials. *J. Hazard. Mater.* **2009**, *163*, 568–577. [[CrossRef](#)] [[PubMed](#)]
5. Mohammadi, N.; Khani, H.; Gupta, V.K.; Amereh, E.; Agarwal, S. Adsorption process of methyl orange dye onto mesoporous carbon material—kinetic and thermodynamic studies. *J. Colloid Interface Sci.* **2011**, *362*, 457–462. [[CrossRef](#)] [[PubMed](#)]
6. Weldegebrieal, G.K. Synthesis method, antibacterial and photocatalytic activity of ZnO nanoparticles for azo dyes in wastewater treatment: A review. *Inorg. Chem. Commun.* **2020**, *120*. [[CrossRef](#)]
7. Pagga, U.; Brown, D. The degradation of dyestuffs: Part II behaviour of dyestuffs in aerobic biodegradation tests. *Chemosphere* **1986**, *15*, 479–491. [[CrossRef](#)]
8. Lin, Y.-C.; Ho, S.-H.; Zhou, Y.; Ren, N. Highly efficient adsorption of dyes by biochar derived from pigments-extracted macroalgae pyrolyzed at different temperature. *Bioresour. Technol.* **2018**, *259*, 104–110.
9. Khadhraoui, M.; Trabelsi, H.; Ksibi, M.; Bouguerra, S.; Elleuch, B. Discoloration and detoxification of a Congo red dye solution by means of ozone treatment for a possible water reuse. *J. Hazard. Mater.* **2009**, *161*, 974–981. [[CrossRef](#)]
10. Mailler, R.; Gasperi, J.; Coquet, Y.; Derome, C.; Buleté, A.; Vulliet, E.; Bressy, A.; Varrault, G.; Chebbo, G.; Rocher, V. Removal of emerging micropollutants from wastewater by activated carbon adsorption: Experimental study of different activated carbons and factors influencing the adsorption of micropollutants in wastewater. *J. Environ. Chem. Eng.* **2016**, *4*, 1102–1109. [[CrossRef](#)]
11. Yao, Y.; Bing, H.; Feifei, X.; Xiaofeng, C. Equilibrium and kinetic studies of methyl orange adsorption on multiwalled carbon nanotubes. *Chem. Eng. J.* **2011**, *170*, 82–89. [[CrossRef](#)]
12. Yang, S.-T.; Chen, S.; Chang, Y.; Cao, A.; Liu, Y.; Wang, H. Removal of methylene blue from aqueous solution by graphene oxide. *J. Colloid Interface Sci.* **2011**, *359*, 24–29. [[CrossRef](#)]
13. Yao, Y.; Miao, S.; Yu, S.; Ping Ma, L.; Sun, H.; Wang, S. Fabrication of Fe<sub>3</sub>O<sub>4</sub>/SiO<sub>2</sub> core/shell nanoparticles attached to graphene oxide and its use as an adsorbent. *J. Colloid Interface Sci.* **2012**, *379*, 20–26. [[CrossRef](#)]
14. Vakili, M.; Cagnetta, G.; Huang, J.; Yu, G.; Yuan, J. Synthesis and regeneration of A MXene-based pollutant adsorbent by mechanochemical methods. *Molecules* **2019**, *24*, 2478. [[CrossRef](#)]
15. Vakili, M.; Zwain, H.M.; Mojiri, A.; Wang, W.; Gholami, F.; Gholami, Z.; Giwa, A.S.; Wang, B.; Cagnetta, G.; Salamatinia, B. Effective adsorption of reactive black 5 onto hybrid hexadecylamine impregnated chitosan-powdered activated carbon beads. *Water* **2020**, *12*, 2242. [[CrossRef](#)]
16. Yuan, M.; Tong, S.; Zhao, S.; Jia, C.Q. Adsorption of polycyclic aromatic hydrocarbons from water using petroleum coke-derived porous carbon. *J. Hazard. Mater.* **2010**, *181*, 1115–1120. [[CrossRef](#)]
17. Liu, X.; Zhang, Y.; Li, Z.; Feng, R.; Zhang, Y. Characterization of corncob-derived biochar and pyrolysis kinetics in comparison with corn stalk and sawdust. *Bioresour. Technol.* **2014**, *170*, 76–82. [[CrossRef](#)]
18. Ahmad, M.; Rajapaksha, A.U.; Lim, J.E.; Zhang, M.; Bolan, N.; Mohan, D.; Vithanage, M.; Lee, S.S.; Ok, Y.S. Biochar as a sorbent for contaminant management in soil and water: A review. *Chemosphere* **2014**, *99*, 19–33. [[CrossRef](#)] [[PubMed](#)]
19. Abdelhafez, A.A.; Li, J. Removal of Pb (II) from aqueous solution by using biochars derived from sugar cane bagasse and orange peel. *J. Taiwan Inst. Chem. Eng.* **2016**, *61*, 367–375. [[CrossRef](#)]
20. Dhillon, S.S.; Gill, R.K.; Gill, S.S.; Singh, M. Studies on the utilization of citrus peel for pectinase production using fungus *Aspergillus Niger*. *Int. J. Environ. Stud.* **2004**, *61*, 199–210. [[CrossRef](#)]
21. Ahiduzzaman, M.; Sadrul Islam, A.K.M. Preparation of porous bio-char and activated carbon from rice husk by leaching ash and chemical activation. *SpringerPlus* **2016**, *5*. [[CrossRef](#)]
22. Wang, H.; Chen, G.; Guo, X.; Abbasi, A.M.; Liu, R.H. Influence of the stage of ripeness on the phytochemical profiles, antioxidant and antiproliferative activities in different parts of *Citrus reticulata* Blanco cv. Chachiensis. *LWT Food Sci. Technol.* **2016**, *69*, 67–75. [[CrossRef](#)]
23. Boluda-Aguilar, M.; García-Vidal, L.; del Pilar González-Castañeda, F.; López-Gómez, A. Mandarin peel wastes pretreatment with steam explosion for bioethanol production. *Bioresour. Technol.* **2010**, *101*, 3506–3513. [[CrossRef](#)] [[PubMed](#)]
24. Unugul, T.; Nigiz, F.U. Synthesis of acid treated carbonized mandarin peel for purification of copper. *Water Pract. Technol.* **2020**, *15*, 460–471. [[CrossRef](#)]
25. Shin, J.; Kwak, J.; Lee, Y.-G.; Kim, S.; Choi, M.; Bae, S.; Lee, S.-H.; Park, Y.; Chon, K. Competitive adsorption of pharmaceuticals in lake water and wastewater effluent by pristine and NaOH-activated biochars from spent coffee wastes: Contribution of hydrophobic and  $\pi$ - $\pi$  interactions. *Environ. Pollut.* **2021**, *270*. [[CrossRef](#)] [[PubMed](#)]
26. Aljerf, L. High-efficiency extraction of bromocresol purple dye and heavy metals as chromium from industrial effluent by adsorption onto a modified surface of zeolite: Kinetics and equilibrium study. *J. Environ. Manag.* **2018**, *225*, 120–132. [[CrossRef](#)]
27. Kumar, P.; Govindaraju, M.; Senthamsilvelvi, S.; Premkumar, K. Photocatalytic degradation of methyl orange dye using silver (Ag) nanoparticles synthesized from *Ulva lactuca*. *Colloids Surf. B Biointerfaces* **2013**, *103*, 658–661. [[CrossRef](#)]

28. Abdi, S.; Nasiri, M. Removal of fast green FCF dye from aqueous solutions using flower gel as a low-cost adsorbent. *Water Sci. Technol.* **2017**, *77*, 1213–1221. [[CrossRef](#)] [[PubMed](#)]
29. Kim, H.; Ko, R.-A.; Lee, S.; Chon, K. Removal efficiencies of manganese and iron using pristine and phosphoric acid pre-treated biochars made from banana peels. *Water* **2020**, *12*, 1173. [[CrossRef](#)]
30. Li, R.; Wang, Z.; Guo, J.; Li, Y.; Zhang, H.; Zhu, J.; Xie, X. Enhanced adsorption of ciprofloxacin by KOH modified biochar derived from potato stems and leaves. *Water Sci. Technol.* **2017**, *77*, 1127–1136. [[CrossRef](#)]
31. Langmuir, I. The adsorption of gases on plane surfaces of glass, mica and platinum. *J. Am. Chem. Soc.* **1918**, *40*, 1361–1403. [[CrossRef](#)]
32. Freundlich, H. *Colloid & Capillary Chemistry*; EP Dutton & Company: Boston, MA, USA, 1922.
33. Tran, H.N.; You, S.-J.; Chao, H.-P. Thermodynamic parameters of cadmium adsorption onto orange peel calculated from various methods: A comparison study. *J. Environ. Chem. Eng.* **2016**, *4*, 2671–2682. [[CrossRef](#)]
34. Tsai, W.-T.; Hsien, K.-J.; Lai, C.-W. Chemical activation of spent diatomaceous earth by alkaline etching in the preparation of mesoporous adsorbents. *Ind. Eng. Chem. Res.* **2004**, *43*, 7513–7520. [[CrossRef](#)]
35. Thommes, M.; Kaneko, K.; Neimark, A.V.; Olivier, J.P.; Rodriguez-Reinoso, F.; Rouquerol, J.; Sing, K.S. Physisorption of gases, with special reference to the evaluation of surface area and pore size distribution (IUPAC Technical Report). *Pure Appl. Chem.* **2015**, *87*, 1051–1069. [[CrossRef](#)]
36. Yorgun, S.; Vural, N.; Demiral, H. Preparation of high-surface area activated carbons from Paulownia wood by ZnCl<sub>2</sub> activation. *Microporous Mesoporous Mater.* **2009**, *122*, 189–194. [[CrossRef](#)]
37. Uğurlu, M.; Gürses, A.; Açıkyıldız, M. Comparison of textile dyeing effluent adsorption on commercial activated carbon and activated carbon prepared from olive stone by ZnCl<sub>2</sub> activation. *Microporous Mesoporous Mater.* **2008**, *111*, 228–235. [[CrossRef](#)]
38. Shin, J.; Lee, S.-H.; Kim, S.; Ochir, D.; Park, Y.; Kim, J.; Lee, Y.-G.; Chon, K. Effects of physicochemical properties of biochar derived from spent coffee grounds and commercial activated carbon on adsorption behavior and mechanisms of strontium ions (Sr<sup>2+</sup>). *Environ. Sci. Pollut. Res.* **2020**. [[CrossRef](#)] [[PubMed](#)]
39. Chon, K.; Cho, J.; Shon, H.K. A pilot-scale hybrid municipal wastewater reclamation system using combined coagulation and disk filtration, ultrafiltration, and reverse osmosis: Removal of nutrients and micropollutants, and characterization of membrane foulants. *Bioresour. Technol.* **2013**, *141*, 109–116. [[CrossRef](#)]
40. Unugul, T.; Nigiz, F.U. Preparation and characterization an active carbon adsorbent from waste mandarin peel and determination of adsorption behavior on removal of synthetic dye solutions. *Water Air Soil Pollut.* **2020**, *231*. [[CrossRef](#)]
41. Chia, C.H.; Gong, B.; Joseph, S.D.; Marjo, C.E.; Munroe, P.; Rich, A.M. Imaging of mineral-enriched biochar by FTIR, Raman and SEM–EDX. *Vib. Spectrosc.* **2012**, *62*, 248–257. [[CrossRef](#)]
42. Chen, T.; Zhou, Z.; Han, R.; Meng, R.; Wang, H.; Lu, W. Adsorption of cadmium by biochar derived from municipal sewage sludge: Impact factors and adsorption mechanism. *Chemosphere* **2015**, *134*, 286–293. [[CrossRef](#)]
43. Mahmoudi, K.; Hamdi, N.; Kriaa, A.; Srasra, E. Adsorption of methyl orange using activated carbon prepared from lignin by ZnCl<sub>2</sub> treatment. *Rus. J. Phys. Chem. A* **2012**, *86*, 1294–1300. [[CrossRef](#)]
44. Son, C.; An, W.; Lee, G.; Jeong, I.; Lee, Y.-G.; Chon, K. Adsorption characteristics of phosphate ions by pristine, CaCl<sub>2</sub> and FeCl<sub>3</sub>-activated biochars originated from tangerine peels. *Separations* **2021**, *8*, 32. [[CrossRef](#)]
45. Lee, Y.-G.; Shin, J.; Kwak, J.; Kim, S.; Son, C.; Cho, K.H.; Chon, K. Effects of NaOH activation on adsorptive removal of herbicides by biochars prepared from ground coffee residues. *Energies* **2021**, *14*, 1297. [[CrossRef](#)]
46. Shin, J.; Lee, Y.-G.; Lee, S.-H.; Kim, S.; Ochir, D.; Park, Y.; Kim, J.; Chon, K. Single and competitive adsorptions of micropollutants using pristine and alkali-modified biochars from spent coffee grounds. *J. Hazard. Mater.* **2020**, *400*. [[CrossRef](#)]
47. Konicki, W.; Aleksandrak, M.; Moszyński, D.; Mijowska, E. Adsorption of anionic azo-dyes from aqueous solutions onto graphene oxide: Equilibrium, kinetic and thermodynamic studies. *J. Colloid Interface Sci.* **2017**, *496*, 188–200. [[CrossRef](#)]
48. Fan, S.; Tang, J.; Wang, Y.; Li, H.; Zhang, H.; Tang, J.; Wang, Z.; Li, X. Biochar prepared from co-pyrolysis of municipal sewage sludge and tea waste for the adsorption of methylene blue from aqueous solutions: Kinetics, isotherm, thermodynamic and mechanism. *J. Mol. Liq.* **2016**, *220*, 432–441. [[CrossRef](#)]
49. Chowdhury, S.; Mishra, R.; Saha, P.; Kushwaha, P. Adsorption thermodynamics, kinetics and isosteric heat of adsorption of malachite green onto chemically modified rice husk. *Desalination* **2011**, *265*, 159–168. [[CrossRef](#)]
50. Esmaeli, A.; Jokar, M.; Kousha, M.; Daneshvar, E.; Zilouei, H.; Karimi, K. Acidic dye wastewater treatment onto a marine macroalga, *Nizamuddina zanardini* (Phylum: *Ochrophyta*). *Chem. Eng. J.* **2013**, *217*, 329–336. [[CrossRef](#)]
51. Elizalde-González, M.; García-Díaz, L. Application of a taguchi L16 orthogonal array for optimizing the removal of acid orange 8 using carbon with a low specific surface area. *Chem. Eng. J.* **2010**, *163*, 55–61. [[CrossRef](#)]